

Application of Digital Lock-in Amplifier in Complex Electromagnetic Interference of Substation

Jiabing Song^{1, 2}, Hengli Song^{1, 2, *}, Xuan Yang^{1, 2}, and Haobin Dong^{1, 2}

Abstract—There is complex electromagnetic interference in the substation. In order to improve detection accuracy, a digital lock-in amplifier is used in the detection of the grounding grid. This paper introduces the principle of non-destructive testing of grounding grid based on electromagnetic method. Firstly, the distribution characteristics of surface magnetic induction intensity at different frequencies are obtained by CDEGS simulation. At the same time, it describes the principle and structure of an orthogonal vector type digital lock-in amplifier in detail. In order to realize the high-precision grounding grid detection system, the hardware circuit of the digital lock-in amplifier is designed by FPGA and analog-to-digital converter. The digital lock-in amplifier algorithm is implemented in the FPGA. Finally, the digital lock-in amplifier is tested. The test results show that when the signal-to-noise ratio of the signal to be tested is -20 dB, the signal amplitude measurement error is less than 3%. The designed digital lock-in amplifier is applied to the actual grounding grid detection, and the topology and corrosion of the grounding network can be detected. Therefore, the digital lock-in amplifier can be effectively applied to non-destructive testing of grounding grid.

1. INTRODUCTION

In a power system, the grounding grid plays a key role in protecting the safety of the power system's operation and the lives of workers. It provides a reference ground for the power system and quickly drains lightning current and fault current, reduces the ground potential rise, and guarantees equipment and personnel safety [1, 2]. With the development of the power system, ultra-high voltage (UHV) large capacity substation has become a trend. Once there is a short circuit fault, the grounding grid cannot timely improve the phenomenon of uneven potential distribution, which will damage the insulation performance of the equipment and endanger the life safety of the staff [3, 4]. Grounding grid fault is an important hidden danger to the safety of the power system. The large area of the grounding grid is buried in the ground, and it is impossible to observe the corrosion degree of the grounding grid intuitively [5]. Therefore, it is necessary to find a detection method that can quickly and effectively find the corrosion area without power outage, in order to detect the corrosion of the grounding grid and ensure the safety of equipment and staff [6, 7]. At the same time, due to the long operation time of many substations, some construction drawings of substation grounding grid are lost, and the corrosion degree and breakpoint of the grounding grid need to be tested. Therefore, it is necessary to carry out non-destructive testing of the grounding grid in the case of unknown topology structure and parameters of the grounding grid.

The equivalent network method relies on the measurement of the conductor resistance of the grounding grid. Its measurement accuracy and detection efficiency are limited, and it needs to know the topology of the grounding grid. The complexity of the topology will also affect the fault diagnosis

Received 10 July 2020, Accepted 27 September 2020, Scheduled 14 October 2020

* Corresponding author: Hengli Song (songhengli@cug.edu.cn).

¹ School of Automation, China University of Geosciences, Wuhan 430074, China. ² Hubei Key Laboratory of Advanced Control and Intelligent Automation for Complex Systems, Wuhan 430074, China.

results. The electrochemical method has the advantages of fast test speed and high test sensitivity, but it can only reflect the corrosion of the ground conductor at the probe position. The main disadvantage of the electromagnetic method is that the electrical equipment and metal structure of the substation will affect its measurement. At the same time, the complex electromagnetic interference problem of the substation must be solved. This paper adopts the non-destructive testing method of grounding grid based on electromagnetic method [8, 9].

There is complex electromagnetic noise in the substation [10]. The interference noise is widely distributed in various frequency bands. The electromagnetic interference is mainly power frequency interference and its odd harmonics. The conductor of the energized grounding grid generates an alternating magnetic field on the ground, and the sensor generates an induced voltage in the alternating magnetic field. The induced voltage in the sensor is very weak compared to the noise, so the receiver needs to design a weak signal detection system. The lock-in amplifier is a weak signal detection instrument commonly used at present and has a wide application space. With the advancement of technology and the emergence of various high-performance digital processors, digital lock-in amplifiers have made great progress. Compared with a traditional analog lock-in amplifier, it has many advantages, such as large dynamic range, good stability, small harmonic distortion, and small temperature drift. The amplitude and phase of the induction signal can be obtained through the digital lock-in amplifier, and the corrosion and breakpoint of the grounding grid can be judged by the amplitude and phase difference.

This paper designs a set of instruments based on a lock-in amplifier. The second section introduces the measurement principle and uses current distribution electromagnetic fields grounding soil structure (CDEGS) analysis to simulate the distribution of magnetic induction intensity on the ground surface of the grounding grid. The third section introduces the design of the instrument and principle of digital lock-in amplifier. The fourth part introduces the realization of digital lock-in amplifier based on field programmable gate array (FPGA). The fifth section includes grounding grid test. The sixth section summarizes the results.

2. THEORY AND SIMULATION

2.1. Principle of Magnetic Field Measurement

Non-destructive testing of substation grounding grid based on electromagnetic method is to inject sinusoidal current into two different ground down conductors in the grounding grid through the transmitter and use the receiving system to detect the distribution of magnetic induction intensity induced on the ground surface. Use the upper-computer software to judge the topological structure of the grounding grid and the location of the fault section.

Flat steel corrosion model is shown in Fig. 1. When the frequency changes, the impedance of the grounding grid will also change due to the skin effect. Considering the skin effect of grounding conductor, conductor resistance is as in following Equation (1). In Equation (1), μ is the permeability, a the conductor radius, ρ the conductor resistivity, and f the current injection frequency. In Equation (2), M is the mutual impedance of the grounding conductor. When the current of a grounding grid changes, the adjacent grounding conductors will produce mutual inductance which affects the distribution of current, where l is the conductor length, d the distance between the two conductors, ρ the soil resistivity, and f the current injection frequency. The impedance of the flat steel is shown in Equation (3), and Equation (4) is the impedance angle.

$$R = \frac{1}{a} \sqrt{\frac{\mu f \rho}{2\pi}} \quad (1)$$

$$M = l\rho_1 \left(\ln \frac{2l}{d} - 1 \right) f \quad (2)$$

$$Z = R_1 + j\omega L + \frac{1}{j\omega c + \frac{1}{R_2}} = \frac{R_2 + R_1 + R_1 R_2^2 \omega^2 C^2 + j(\omega L + \omega^3 L R_2^2 C^2 - R_2^2 \omega C)}{1 + R_2^2 \omega^2 C^2} \quad (3)$$

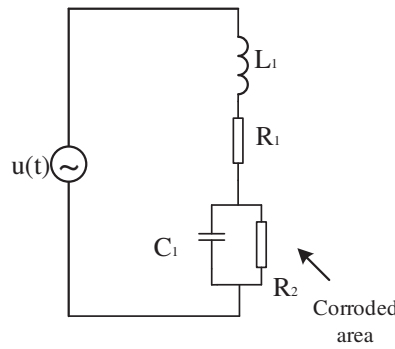


Figure 1. Flat steel corrosion model.

$$\theta_1 = \arctan \frac{\omega L + \omega^3 L R_2^2 C^2 - R_2^2 \omega C}{R_2 + R_1 + R_1 R_2^2 \omega^2 C^2} \tag{4}$$

According to Biot Savart Law, the magnitude of the magnetic induction intensity dB generated by the current element $I dl$ at a certain point P in space is proportional to the magnitude of the current element $I dl$ and proportional to the sine of the angle between the direction of current element $I dl$ and the direction of the $I dl$ to point P. It is inversely proportional to the square of the distance from the current element $I dl$ to point P, which is:

$$dB = \frac{\mu}{4\pi} \frac{I dl \sin \theta}{r^2} \tag{5}$$

From this, the magnetic induction intensity dB of the current-carrying straight conductor of a certain length at any point P outside the straight conductor can be inferred. Take the cylindrical coordinate system and take the straight conductor as the y -axis, the current flow direction along the $+y$ axis (\vec{a}_r), and the midpoint of the conductor as the coordinate origin, as shown in Fig. 2.

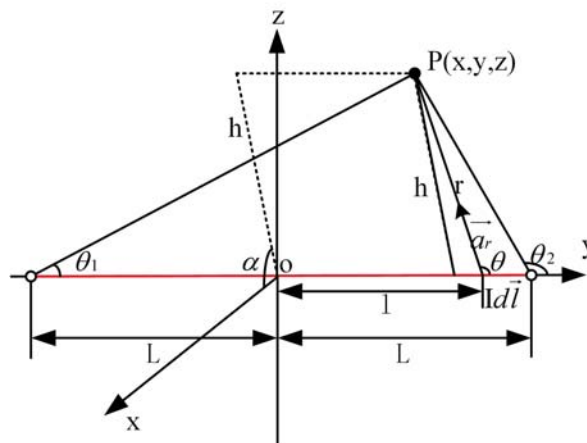


Figure 2. Magnetic field analysis of current-carrying conductor.

In Equation (6), θ_1 and θ_2 are marked in Fig. 2. h is the distance from the field point $P(x, y, z)$ to the y -axis. The direction of the magnetic field of each current element on the straight conductor at point P is perpendicular to the plane where the straight conductor and point P are located, denoted as \vec{a}_α . The magnetic induction intensity by the straight conductor current at point $P(x, y, z)$ is

$$\vec{B} = \vec{a}_\alpha \frac{\mu I}{4\pi h} (\cos \theta_1 - \cos \theta_2) \tag{6}$$

According to the above analysis, the magnetic induction intensity at a certain point in space is related to the position of the conductor and the current flowing through it.

2.2. Simulation Analysis of Grounding Grid Based on CDEGS

2.2.1. Grounding Grid Simulation Model

Use the SesCAD tool to build the topology structure of the grounding grid as shown in Fig. 3. The six grounding conductors in the X and Y directions are equivalent to a cylinder, each of which is 15 m long and 3 cm in diameter, and each conductor is divided into five parts. The relative resistivity of the grounding conductor is $1.78 \times 10^{-7} \Omega \cdot \text{m}$ and a relative magnetic permeability of 200. Inject sine wave current of certain amplitude and frequency is from point A(0, 0) and point C(15, 0). The red dot in the figure represents 1 cm of fracture; the red line represents the corrosion area; and the corrosion length is 2 m. A single measuring line $y = 2 \text{ m}$ is shown in the blue line in Fig. 3.

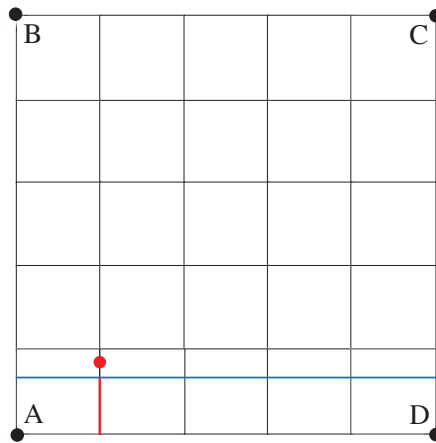


Figure 3. Schematic diagram of the grounding grid model.

Use the MALZ module in CDEGS to simulate the magnetic induction intensity of the grounded grid and inject 10 A, 1.25 kHz sinusoidal excitation current from points A(0, 0) and C(15, 15) in the grounding grid model. A two-layer soil model is selected. The first layer has a thickness of 5 meters. The soil has a resistivity of $80 \Omega \cdot \text{m}$; the second layer has an infinite thickness; and the soil resistivity is $200 \Omega \cdot \text{m}$. The surface magnetic induction intensity distribution color block diagram is as shown in Fig. 4. It is to clearly distinguish the topological structure of the grounding grid.

2.2.2. Effect of Excitation Frequency on Surface Magnetic Induction

Based on the grounding grid model in Fig. 3, inject 10 A sine wave current at points A and C of the model. The frequency range is 10 Hz to 10 MHz. The soil structure is set to a two-layer model. The magnetic induction intensity changes with frequency as shown in Fig. 5. In this simulation, it can be seen that the influence of excitation current frequency in 10 Hz–100 kHz on the surface magnetic induction intensity is very small, and the influence is gradually larger above 100 kHz.

2.2.3. Influence of Soil Structure on Magnetic Induction Intensity

In different regions, soil resistivity is different, and the difference in soil moisture content will also lead to changes in resistivity [9]. Therefore, it is necessary to analyze the change of magnetic induction intensity on the surface of the grounding grid under different soil structures. In the substation, 10–20 cm cement will be laid on the ground, and the resistivity of the cement is more than $2000 \Omega \cdot \text{m}$, so it is necessary to study the influence of the high resistivity layer on the actual test. Set the soil structure as shown in Table 1, and the magnetic induction intensity distribution on the ground surface obtained

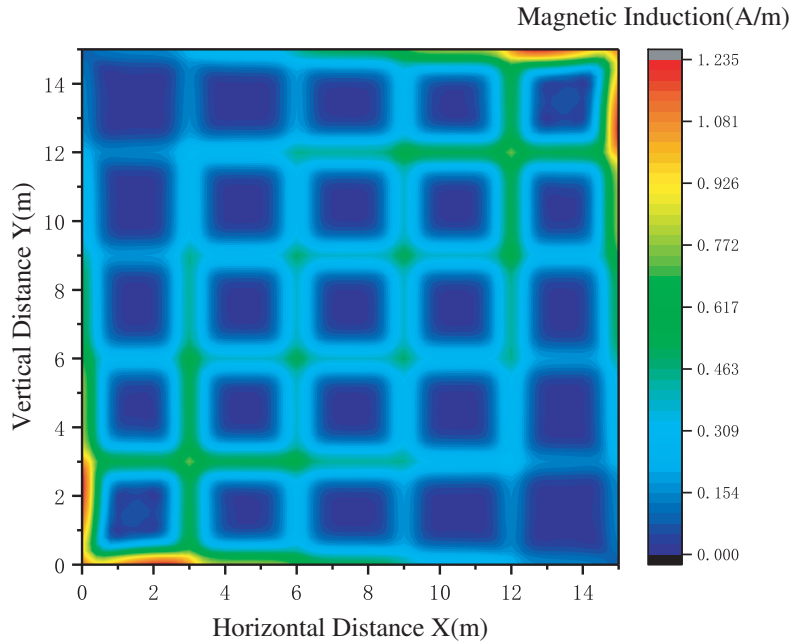


Figure 4. Distribution of magnetic induction intensity on the ground surface.

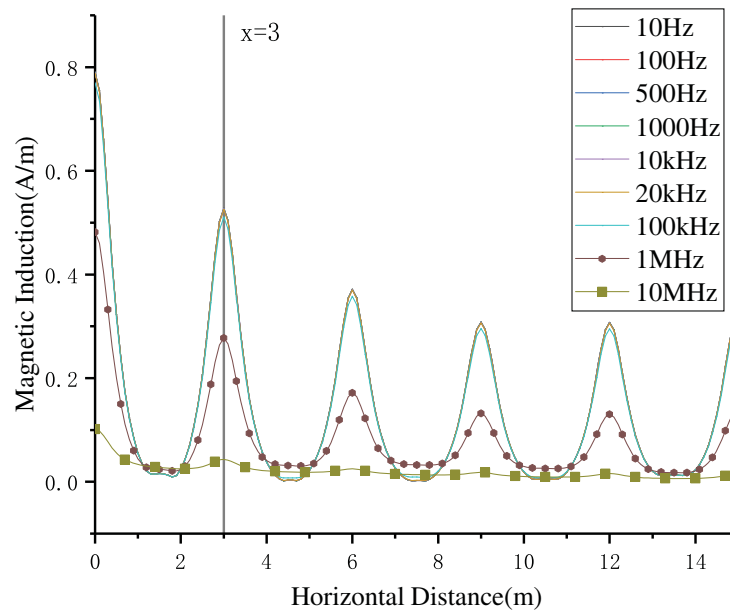


Figure 5. The curve of the magnetic induction intensity with frequency.

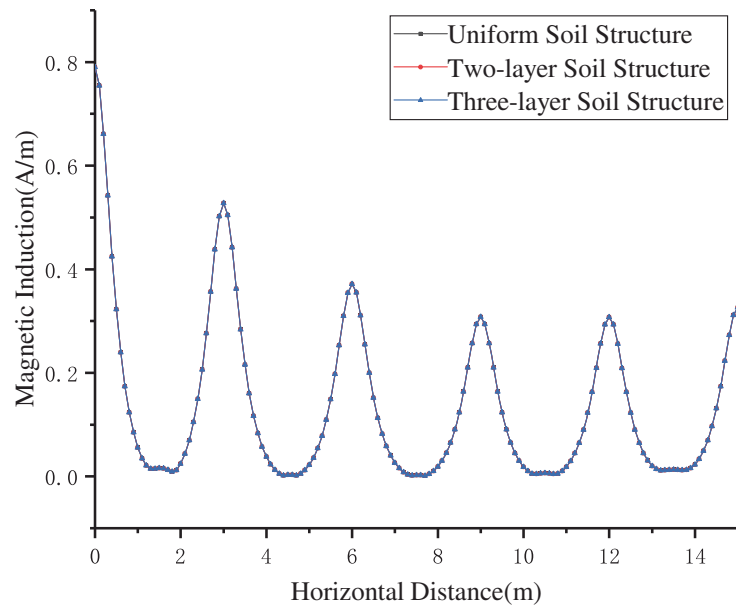
by simulation is shown in Fig. 6. It can be concluded that the magnetic induction intensity waveforms of the three soil structures are almost identical. When the current is injected directly into the grounding grid, because the resistivity of the grounding conductor is far less than that of the soil, the current is mainly distributed in the grounding conductor, and the influence of soil resistivity can be ignored.

2.2.4. Effect of Flat Steel Corrosion on the Surface Magnetic Induction Intensity

The grounding grid model is established as shown in Fig. 3. It is assumed that only the resistance value will be affected after the grounding grid is corroded, and four different degrees of corrosion are

Table 1. Three soil structure parameters.

Number of soil layers	Soil resistivity ($\Omega \cdot \text{m}$)	Thickness (m)
1-1	100	∞
2-1	100	5
2-2	200	∞
3-1	2000	0.1
3-2	100	5
3-3	200	∞

**Figure 6.** Distribution of magnetic induction intensity under different soil structures.

set. The corrosion parameters are shown in Table 2. When $y = 2$, the magnetic induction intensity of x from 0 to 5 is shown in Fig. 7. It can be seen from the figure that the magnetic induction intensity of mild corrosion conductor is 78% of an uncorroded conductor, and the change is small at this time. The moderate corrosion magnetic field is 64.4% of an uncorroded conductor. Magnetic induction intensity changes significantly during severe corrosion. The magnetic induction intensity changes significantly during severe corrosion, and it drops to 16% of normal. When the conductor breaks, the magnetic induction intensity is close to 0. It is easy to judge the severe corrosion and fracture conductors in the actual test, and the mild and moderate corrosion needs further processing because the change is not obvious.

Table 2. Corrosion parameter settings.

Degree of corrosion	Corrosion length (m)	Corrosion conductor diameter (m)
Mild	2	0.025
Moderate	2	0.015
Severe	2	0.005
fracture	2	0

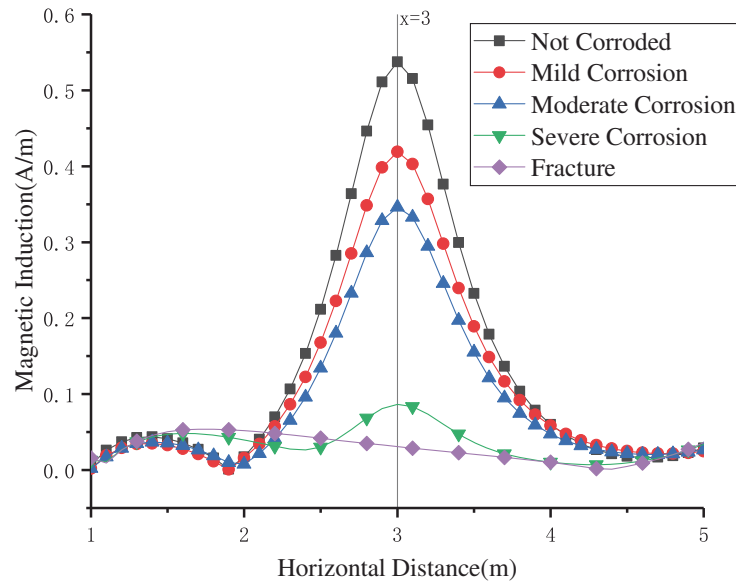


Figure 7. Magnetic induction intensity distribution under different corrosion conditions.

3. MEASURING SYSTEM DESIGN AND PRINCIPLE OF DIGITAL LOCK-IN ALGORITHM

3.1. Instrument Design

3.1.1. Instrument Transmitter Design

The transmitter block diagram is shown in Fig. 8. The receiver and transmitter need to synchronize the phase of the excitation signal and frequency communication to ensure that the two signals have the same frequency phase. The MCU (Micro Control Unit) generates signals with different frequencies and amplitudes through DAC. Programmable amplifier can further adjust the amplitude of the transmission signals. The power amplifier can convert the small voltage signals transmitted into current signals. The feedback loop automatically adjusts the power by collecting the feedback voltage through ADC. The output frequency is between 100 Hz and 10 kHz. The output amplitude is 0 ~ 5 V.

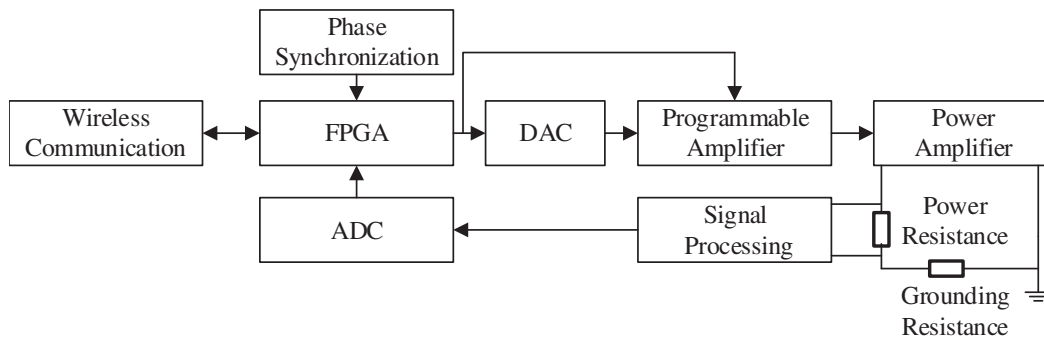


Figure 8. Transmitter design block diagram.

3.1.2. Instrument Receiver Design

The receiver block diagram is shown in Fig. 9. The receiver includes GPS triggered acquisition, wireless synchronization reference signal, sensor automatically adjusting resonance frequency, signal processing, and host computer storage display.

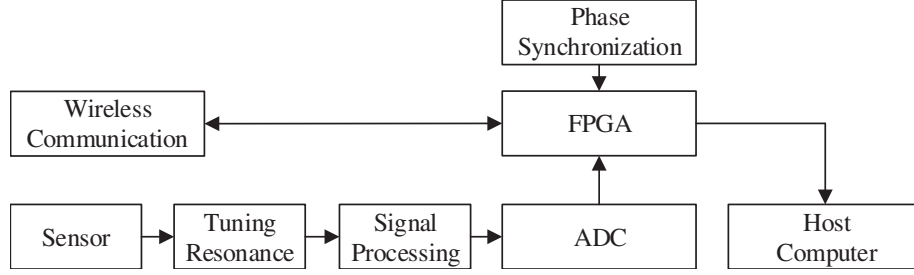


Figure 9. Receiver design block diagram.

3.2. Principle of Digital Lock-in Algorithm

The lock-in amplifier technology is a detection method that uses the principle of cross-correlation of the measured signal and the reference signal to narrow-band the signal, removes unwanted noise signals, and extracts effective information.

3.2.1. Cross-Correlation Detection

The principle of cross-correlation detection is to multiply the signal to be tested by the reference signal and then output it through an integrator or filter. Let the signal to be tested be:

$$x(t) = s(t) + n(t) = A \sin(\omega_0 t + \phi) + N(t) \quad (7)$$

The reference signal has an angular frequency of ω_1 and a sinusoidal signal with an initial phase of ϕ_0

$$y(t) = B \sin(\omega_1 t + \phi_0) \quad (8)$$

After processing by the correlator, the result is

$$\begin{aligned} R(t) &= \int_{t_0}^{t_1} x(t)y(t)dt \\ &= \frac{1}{2}AB \int_{t_0}^{t_1} \{ \cos[(\omega_0 - \omega_1)t + \phi - \phi_0] - \cos[(\omega_0 + \omega_1)t + \phi + \phi_0] \} dt + \int_{t_0}^{t_1} BN(t) \sin(\omega_1 t + \phi_0) dt \end{aligned} \quad (9)$$

The former part of the equation is the cross-correlation output of the useful signal and the reference signal, followed by the cross-correlation output of the noise and reference signal. When the reference signal frequency is equal to the useful signal frequency, which is $\omega_0 = \omega_1$, and the initial phase of the reference signal is 0, the output of the final useful signal and reference signal is passed through a series of transformations:

$$R(t) = \frac{AB(t_1 - t_0)}{2} \cos(\phi) \quad (10)$$

$R(t)$ is a DC signal. The larger $R(t)$ is, the larger the signal to be measured is. When the phase difference is zero, its amplitude is the largest.

3.2.2. Lock-in Amplifier Working Principle

The lock-in amplifier is a weak signal detection device designed by cross-correlation detection in the correlation principle. It consists of a phase detector, a signal channel, a reference channel, etc., and its working principle is shown in Fig. 10. The analog signal to be tested first needs the ADC module to perform analog-to-digital conversion. The two orthogonal reference signals are generated by the numerically controlled oscillator. After the signal to be tested and the reference signal passes through the phase detector and filter, the output of the useful signal is obtained. The lock-in amplifier mainly utilizes the relationship between the reference signal and measured signal, and uses phase locking technology to compress the noise bandwidth to limit the noise, thereby detecting the amplitude and phase of the periodic and repetitive signal.

The cross-correlation output of the single-channel useful signal and reference signal cannot be kept constant. In actual operation, in order to accurately measure the amplitude and phase of the signal, the phase of the reference signal is shifted by 90° , and the two-channel digital correlation detection, which is the orthogonal vector, is used.

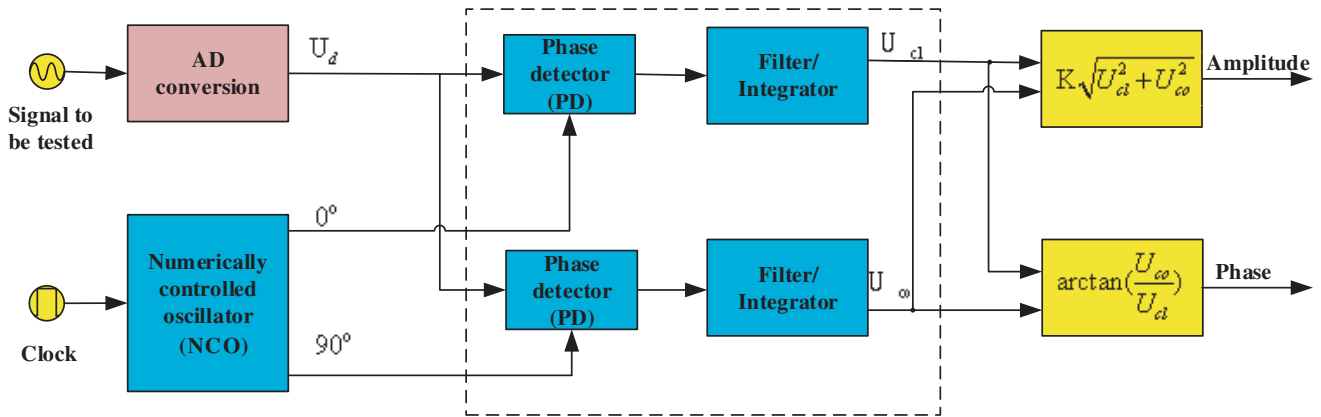


Figure 10. Lock-in amplifier calculation schematic.

4. IMPLEMENTATION BASED ON FPGA PLATFORM

In the grounding grid detection system, the overall block diagram of the designed digital lock-in amplifier is shown in Fig. 11. The system includes a signal conditioning circuit, a low noise preamplifier, a programmable filter, an ADC acquisition chip, an FPGA, etc. The working process is: The reference square wave signal is internally generated by the FPGA and input to the signal conditioning circuit. The signal conditioning circuit generates a sine wave signal of the same frequency as the reference square wave and injects into the grounding grid conductor, and the grounding conductor that conducts the current generates an induced magnetic field; the coil induced voltage measured by the sensor is preamplified, filtered, and converted into a dual modulated voltage signal. The ADC acquisition chip converts the analog signal into a digital signal, then sends it to the FPGA, and performs digital demodulation and digital low-pass filtering in the FPGA to obtain effective two-way information. In the digital lock-in

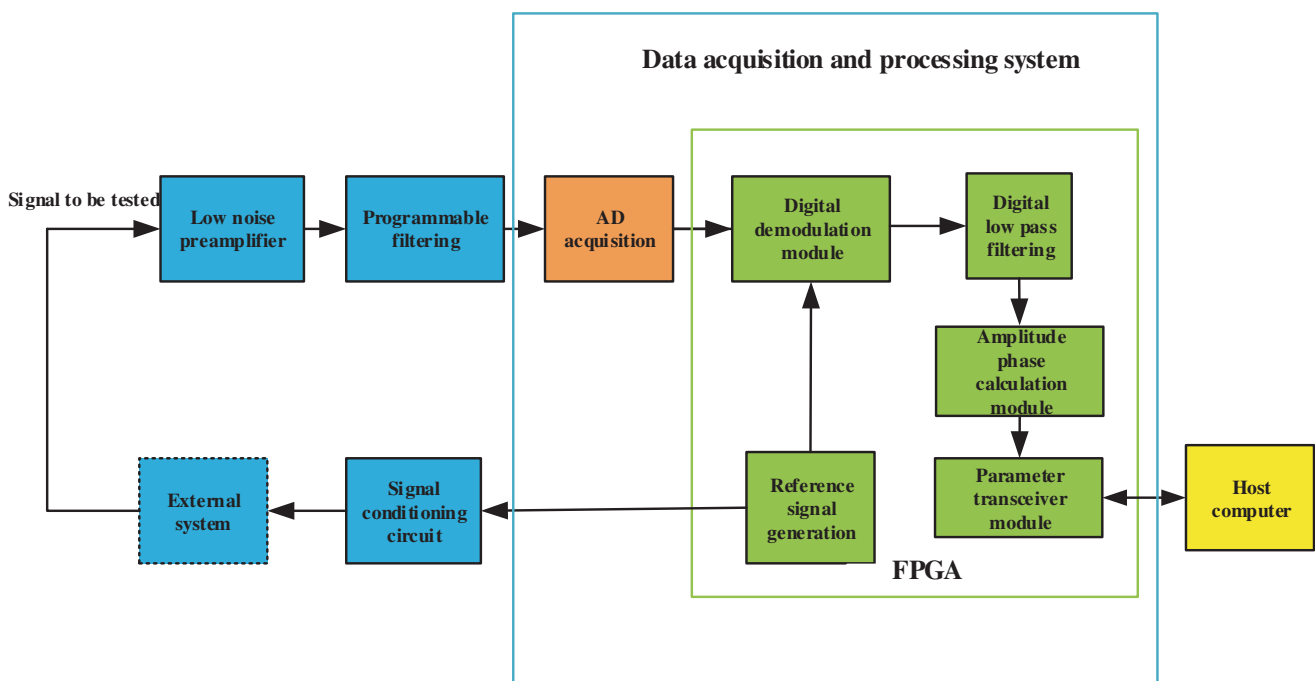


Figure 11. Overall block diagram of a digital lock-in amplifier.

amplification system, the core technology lies in ADC acquisition, digital correlation demodulation and digital filtering algorithms.

The software design of the data acquisition and processing system mainly includes FPGA design of AD7606 acquisition chip control, digital demodulation related algorithm, amplitude and phase calculation module, and parameter transceiver module.

4.1. AD7606 Control Design

In order to realize communication with the ADC conversion chip, an ADC control module is designed. The ADC chip selected in this paper is AD7606. AD7606 is a 16-bit, eight-channel, high-precision analog-to-digital converter with eight channels independent of each other, simultaneous sampling, a maximum sample rate of 200kSPS, and a built-in digital filter with linear phase. According to the conversion timing diagram of AD7606, the corresponding control module is designed in FPGA.

4.2. Digital Correlation Demodulation Module Design

The correlation demodulator is the core component of the lock-in amplifier. The general correlation demodulator consists of a multiplier and a low-pass filter. In this paper, square wave is used as the reference signal of the lock-in amplifier. The multiplication of the signal to be measured with the square wave is essentially the transformation of the symbol (Square wave with a maximum value of 1 V and a minimum of -1 V, multiplying the measured signal by 1 will not change the value and symbol, and that multiplying by -1 will reverse the symbol), so that the multiplier can be replaced by an adder. The accumulator is used to eliminate the AC signal, thereby replacing the low pass filter.

The AD7606 module collects a set of data and then performs symbol conversion according to the level of the two reference signals (the reference signal is unchanged for the high level symbol, and the low level is inverted) and is accumulated and then averaged to `sum1_ave` and `sum2_ave`. Square the two average values and add them to `sum_all`, and the data obtained after the `sum_all` square root operation are linear with the peak value of the original input data. Since Verilog cannot directly implement the square root operation, the square root algorithm is required to write the module of the square root operation.

4.3. Amplitude Phase Calculation Module Design

The amplitude phase calculation module is used to complete the division and square sum root number operation of the two DC signals, thereby obtaining the amplitude phase information of the signal to be tested. The implementation of the amplitude calculation is to first complete the square operation of the two signals by the two DC quantities, then calculate the sum of the two data by the adder, and finally use the successive approximation algorithm to perform the square operation. The two channels of DC are divided to obtain a tangent (or inverse tangent) of the phase difference between the signal to be tested and the reference signal.

The successive approximation algorithm flow is shown in Fig. 12. First, the data are input into data `[15 : 0]`, then the experimental value `D_z [7 : 0]` and the determined value `D_q [7 : 0]` are set, and in

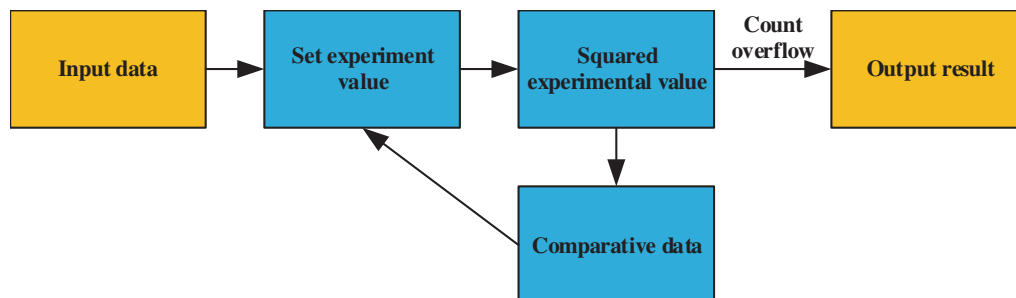


Figure 12. Successive approximation algorithm block diagram.

order from high to low. Set each bit to 1 in turn (e.g., D_z [7] is set to 1), then square the experimental value, and compare it with the input data. If the square of the experimental value is greater than the input value ($D_z^2 > data$), then this bit is 0 (D_q [7] is 0), and vice versa ($D_z^2 \leq data$), this bit is 1 (D_q [7] is 1); iterate to the last bit. It can be seen that if it is n bit data, then $n/2$ iterations are needed, and if one cycle is calculated each time, $n/2$ cycles are required.

4.4. Parameter Transceiver Module

The data obtained after the square operation are a 16 bit wide hexadecimal number. It needs to be converted into multiple 8-bit strings and printed into the serial port. First, convert the hexadecimal number to 8421 BCD code. The 16 bit wide hexadecimal number is converted to a decimal number of up to 65535, and the first to fifth digits of the number are represented by five 4 bit wide BCD codes. Convert the corresponding value of the BCD code into the ascii code and transfer it to the host computer through the serial port. The host computer will display the decimal data for the user to view. When the input data TX_Data is updated, the trigger is enabled to start a byte serial output. Each 16 bit wide hexadecimal number needs to be transmitted in 5 bytes.

5. APPLICATION IN GROUNDING GRID DETECTION

5.1. System Overview

Grounding grid non-destructive testing system application background as shown in Fig. 13, the system is mainly composed of a receiver, a transmitter, power amplification, a host computer, etc.

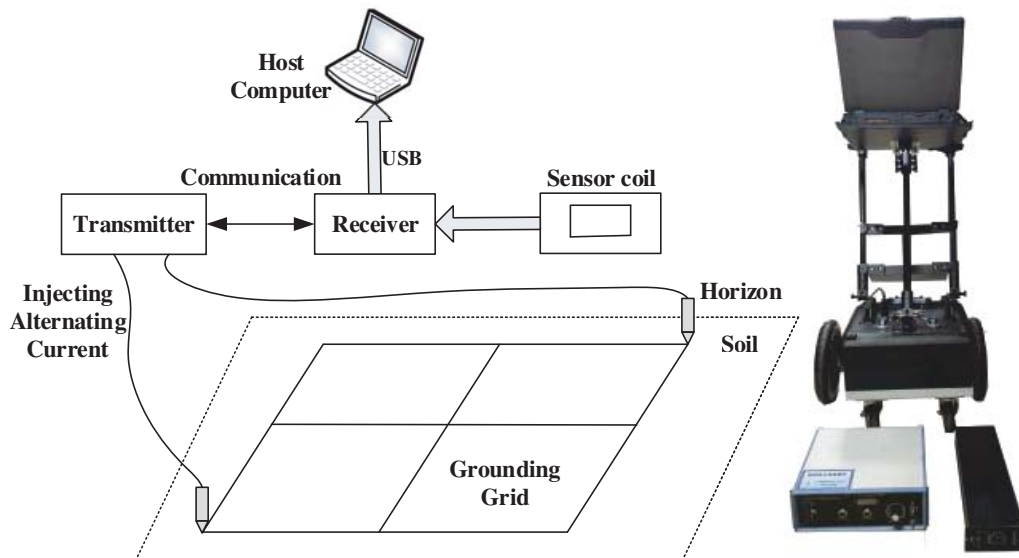


Figure 13. Composition and application of non-destructive tester for grounding grid.

In the grounding grid non-destructive testing system, the receiver part is mainly used for the generation of the reference signal and the amplitude and phase measurement of the signal to be tested, and is mainly composed of an ADC acquisition module and an FPGA digital lock-in amplifier. The working process of the grounding grid non-destructive testing system is: a square wave signal with a certain frequency and a duty cycle of 50% is internally generated by the FPGA and injected into the synchronous signal end of the transmitter; the transmitter injects a sine wave signal of the same frequency as the reference signal into the grounding grid. A grounding conductor that conducts current produces an induced magnetic field. The coil induced voltage measured by the sensor is filtered, ADC converted and sent to the signal calculation module in the receiver, and finally the amplitude and phase of the induced voltage are calculated.

5.2. Experiment and Verification

Applying the designed digital lock-in amplifier to the grounding grid for non-destructive testing first needs to verify that it can correctly measure the amplitude of the sinusoidal signal. A signal generator is used to output a sinusoidal signal of a certain frequency and then sampled by ADC, and the input signal is demodulated by a lock-in amplifier, and the relationship between the demodulated output result and the actual amplitude of the output is compared. The signal generator output frequency is 1.25 kHz, and the amplitude is between 500 mVpp and 6500 mVpp. Ten tests are performed. The test results are shown in Table 3. It can be concluded from the table that the relative error of the amplitude of the digital lock-in amplifier is less than 3%, which satisfies the requirements of grounding grid detection for amplitude calculation.

Table 3. Digital lock-in amplifier amplitude measurement.

Signal amplitude to be measured (mVpp)	Lock-in amplifier output (mVpp)	Relative error
632	649	2.63%
950	967	1.82%
1420	1405	1.08%
1920	1918	0.11%
2480	2495	0.62%
3140	3109	0.98%
3840	3791	1.26%
4740	4765	0.53%
5500	5531	0.57%
6340	6333	0.11%

Due to the complex electromagnetic environment of the substation, a large amount of noise is often mixed in the signal to be tested. Therefore, the digital lock-in amplifier applied to the substation grounding grid detection should have good noise suppression capability. The signal generator is used to generate a white noise signal, which is superimposed with the effective signal output by the transmitter and sent to the digital lock-in amplifier for amplitude calculation. The results are shown in Table 4. It can be obtained that when the signal-to-noise ratio of the signal to be tested is -20 dB, the relative error of the amplitude of the digital lock-in amplifier is less than 3%, which satisfies the requirement of noise suppression for grounding network detection.

Table 4. Noise suppression test.

Signal amplitude (mVpp)	Noise amplitude (mVpp)	Lock-in amplifier output amplitude (mVpp)	Relative error
1000	0	1068	\
1000	50	1068	0
1000	1000	1072	0.37%
1000	5000	1092	2.25%
1000	10000	1100	3.00%

5.3. Determination of the Topology of the Grounding Network

Lay a square grounding grid with a length and width of 4 meters. Replace the flat steel with a conductive copper wire and add a transverse wire and a longitudinal wire in the middle. Firstly, the

sine wave current is injected into the diagonal of the grounding grid through the transmitter and the measurement system is turned on. Then the receiver measures the magnetic induction intensity above the grounding grid. Finally, the measurement results are saved to the upper computer. The magnetic induction intensity distribution of the host computer is shown in Fig. 14. The conductor topology can be inferred from Fig. 14. It is concluded that the designed grounding grid non-destructive detector can accurately measure the topology of the grounding grid conductor within the allowable range of the actual measurement error.

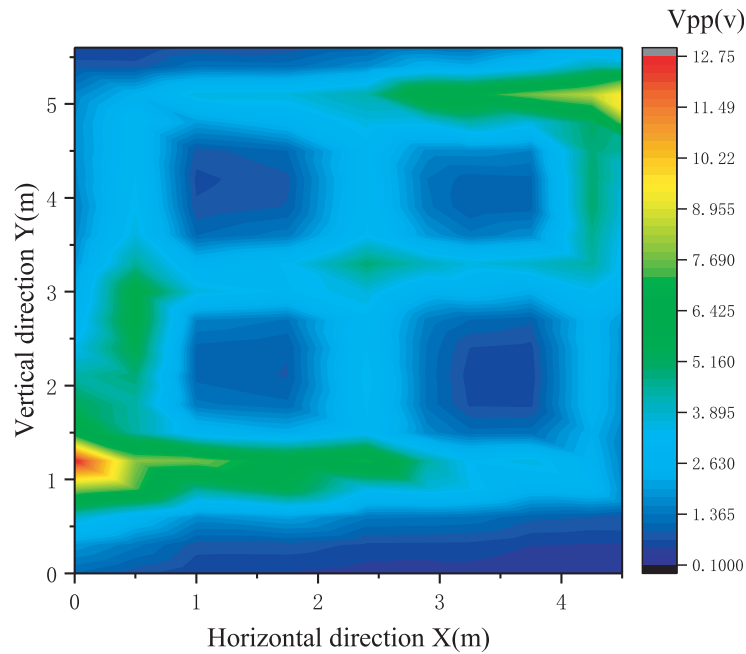


Figure 14. Distribution of magnetic induction intensity on the surface.

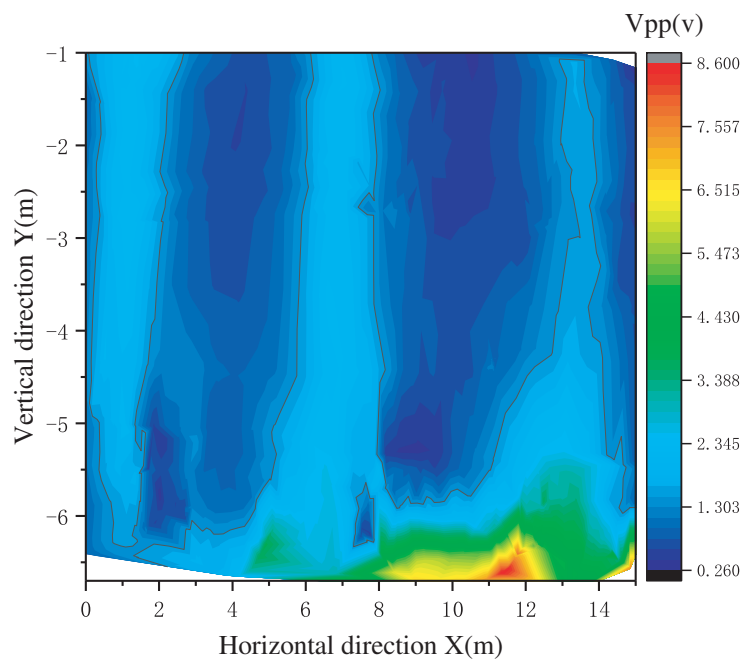


Figure 15. Topological structure diagram of substation grounding grid.

5.4. Actual test of substation

In order to verify the detection effect of the non-destructive tester in the actual substation, the test was carried out in a 220 kV substation in a certain city. During the test, the substation operated normally. The surface magnetic induction intensity is shown in Fig. 15. Fig. 16 is the amplitude and phase change curve of $y = 1.8$ magnetic induction intensity. The topological structure of the grounding grid can be clearly seen from Fig. 15, and the flat steel on the right side is severely corroded. It can be seen from Fig. 16 that the amplitude and phase of the flat steel on the right have a smaller change than the flat steel on the left, so it can be inferred that the flat steel is corroded.

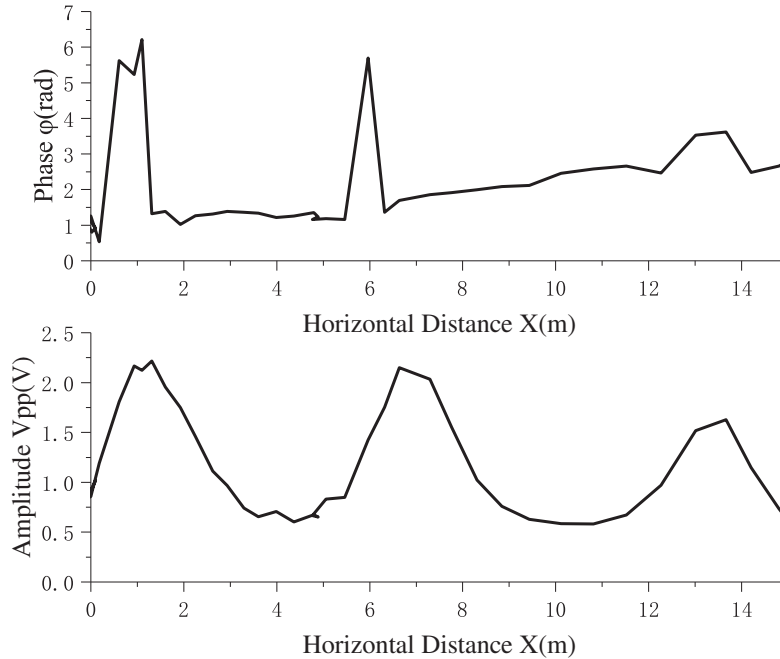


Figure 16. Change curve of amplitude and phase when $y = 1.8$.

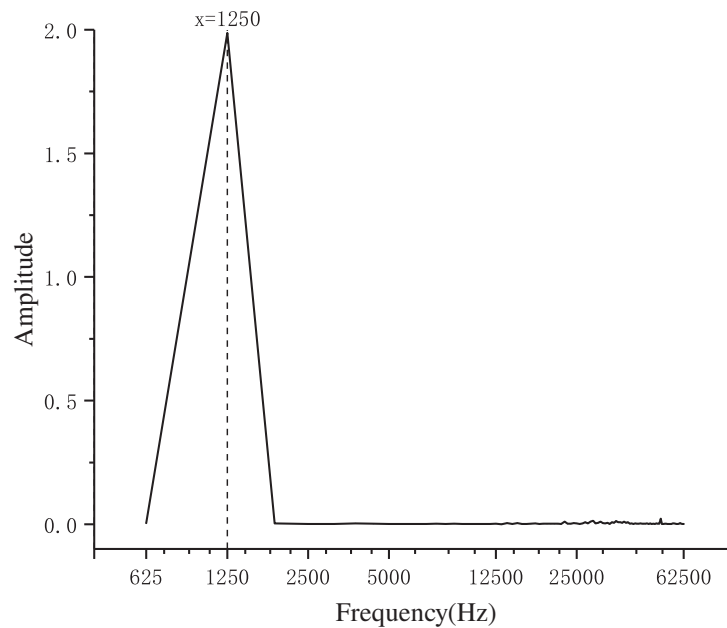


Figure 17. FFT spectrum image of signal.

5.5. Analysis of Grounding Grid Noise

In order to check the magnitude of the environmental noise interference, the magnetic induction intensity above the flat steel was measured in the laboratory. Send the data collected by ADC to the host computer and perform fast Fourier transform (FFT) analysis on the data. As shown in Fig. 17, the SFDR value is 87.6. Since the signal has been low-pass filtered, the signal is better.

6. CONCLUSION

In this paper, the design scheme of digital lock-in amplifier based on FPGA is proposed. The grounding grid non-destructive testing system based on FPGA digital lock-in amplifier is developed and applied to grounding grid non-destructive testing. Firstly, the surface magnetic induction intensity characteristics are obtained by using CDEGS simulation. This can provide theoretical support for the actual test system. The following research results are obtained: For the pure resistance network, the optimal excitation current frequency range is found, which is below 100 kHz; when the grounding grid is corroded, the surface magnetic induction intensity will become smaller. Finally, a set of instruments is designed, and the transmitter mainly includes the signal generating circuit of FPGA and the feedback circuit to ensure the signal amplitude stability. The receiver includes a sensor receiving circuit, a lock-in amplifier, and an upper computer display. At the end of this article, the grounding grid is tested, which can clearly distinguish the topology. Since there is no easy-to-use and easy-to-form instrument in the field of non-destructive testing of grounding grids, this system solution has great application value in practical products.

ACKNOWLEDGMENT

This work was Financially Supported in part by the Foundation of Wuhan Science and Technology Bureau under Grant 2017010201010142, and in part by the Foundation of Science and Technology on Near-Surface Detection Laboratory under Grant TCGZ2017A001.

REFERENCES

1. Yang, X., H. Dong, and H. Song, "Non-destructive testing method for substation grounding grid based on electromagnetic method," *IEEE International Instrumentation and Measurement Technology Conference (I2MTC)*, 1–5, 2019.
2. Wang, X., Z. Fu, Y. Wang, et al., "A non-destructive testing method for fault detection of substation grounding grids," *Sensors*, Vol. 19, No. 9, 2046.
3. Hu, J., J. Hu, D. Lan, et al., "Corrosion evaluation of the grounding grid in transformer substation using electrical impedance tomography technology," *IECON 2017-43rd Annual Conference of the IEEE Industrial Electronics Society IEEE*, 5033–5038, 2017.
4. Visacro, S., R. Alipio, C. Pereira, et al., "Lightning response of grounding grids: simulated and experimental results," *IEEE Transactions on Electromagnetic Compatibility*, Vol. 57, No. 1, 121–127, 2015.
5. Li, X., F. Yang, J. Ming, et al., "Imaging the corrosion in grounding grid branch with inner-source electrical impedance tomography," *Energies*, Vol. 11, No. 7, 2018.
6. Wu, X., X. Zhang, J. Hao, et al., "A smart detection system for power grounding grid based on GPR," *First International Conference on Information Sciences, Machinery, Materials and Energy*, Atlantis Press, 2015.
7. Yu, C., Z. Fu, Q. Wang, et al., "A novel method for fault diagnosis of grounding grids," *IEEE Transactions on Industry Applications*, Vol. 51, No. 6, 5182–5188, 2015.
8. Fu, Z., X. Wang, Q. Wang, et al., "Advances and challenges of corrosion and topology detection of grounding grid," *Applied Sciences*, Vol. 9, No. 11, 2290, 2019.

9. Song, H., H. Dong, and P. Zhang, "A virtual instrument for diagnosis to substation grounding grids in harsh electromagnetic environment," *IEEE International Instrumentation and Measurement Technology Conference (I2MTC)*, 1–6, 2017.
10. Safigianni, A. S., "Christina Tsompanidou G. Measurements of electric and magnetic fields due to operation of indoor power distribution substations," *IEEE Trans. on Power Delivery*, Vol. 20, No. 3, 1800–1805, 2005.